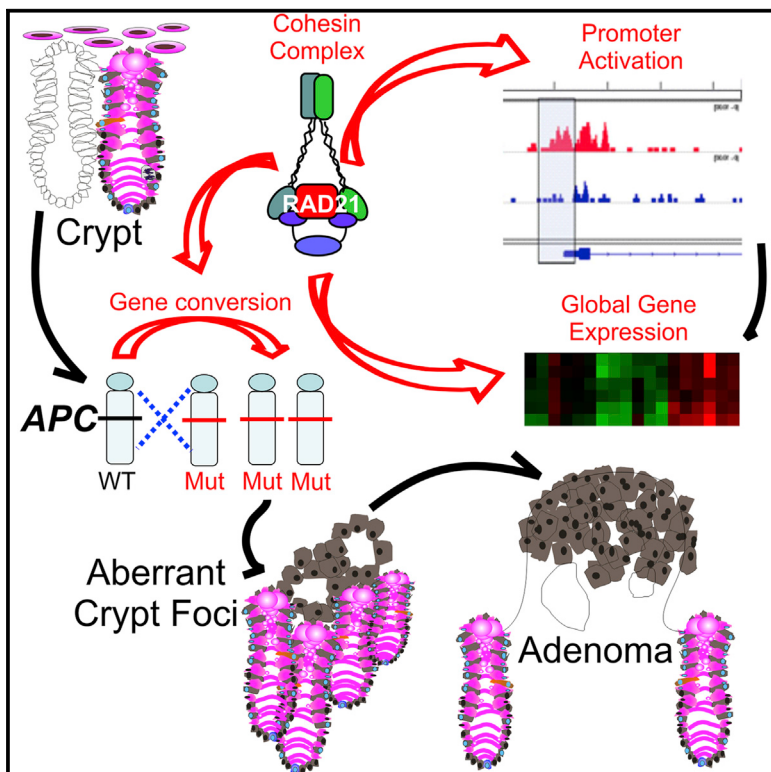


# Cohesin Rad21 Mediates Loss of Heterozygosity and Is Upregulated via Wnt Promoting Transcriptional Dysregulation in Gastrointestinal Tumors

## Graphical Abstract



## Authors

Huiling Xu, Yuqian Yan, ..., Michael J. McKay, Robert G. Ramsay

## Correspondence

[rob.ramsay@petermac.org](mailto:rob.ramsay@petermac.org)

## In Brief

Rad21 holds the cohesin complex together as part of its role in chromosome partitioning and DNA repair. Xu et al. identify Rad21 as a key mediator of *Apc* gene heterozygous loss, the event initiating intestinal tumorigenesis. The subsequent activation of the Wnt pathway further induces Rad21, global gene dysregulation, chromosome instability, and pervasive retrotransposon activation.

## Highlights

Rad21 is identified as a critical mediator of *Apc*<sup>WT</sup> LOH

LOH and CIN are formally documented in vitro in primary intestinal cells

Rad21 regulates key CRC-associated genes

Rad21 is identified as a key driver of L1 retrotransposon expression

## Accession Numbers

GSE59283



# Cohesin Rad21 Mediates Loss of Heterozygosity and Is Upregulated via Wnt Promoting Transcriptional Dysregulation in Gastrointestinal Tumors

Huiling Xu,<sup>1,2,3,12</sup> Yuqian Yan,<sup>1,12</sup> Siddhartha Deb,<sup>4,5</sup> Danny Rangasamy,<sup>6</sup> Markus Germann,<sup>1,2</sup> Jordane Malaterre,<sup>1,2</sup> Noreen C. Eder,<sup>1</sup> Robyn L. Ward,<sup>7</sup> Nicholas J. Hawkins,<sup>8</sup> Richard W. Tothill,<sup>9</sup> Long Chen,<sup>6</sup> Neil J. Mortensen,<sup>10</sup> Stephen B. Fox,<sup>3,4</sup> Michael J. McKay,<sup>11</sup> and Robert G. Ramsay<sup>1,2,\*</sup>

<sup>1</sup>Differentiation and Transcription Laboratory, Peter MacCallum Cancer Centre (PMCC), East Melbourne, VIC 3002, Australia

<sup>2</sup>Sir Peter MacCallum Department of Oncology, The University of Melbourne, Parkville, VIC 3000, Australia

<sup>3</sup>Department of Pathology, The University of Melbourne, Parkville, VIC 3000, Australia

<sup>4</sup>Pathology Department, PMCC, East Melbourne, VIC 3002, Australia

<sup>5</sup>Victorian Cancer Biobank, Carlton, VIC 3053, Australia

<sup>6</sup>John Curtin School of Medical Research, The Australian National University, Acton, ACT 2601, Australia

<sup>7</sup>Prince of Wales Clinical School, University of New South Wales (UNSW), Sydney, NSW 2052, Australia

<sup>8</sup>School of Medical Sciences, UNSW, Sydney, NSW 2052, Australia

<sup>9</sup>Cancer Therapeutics Program, Cancer Research Division, PMCC, East Melbourne, VIC 3002, Australia

<sup>10</sup>Department of Colorectal Surgery, Oxford University Hospitals, Oxford Cancer Centre, Churchill Hospital, Oxford OX3 7LJ, UK

<sup>11</sup>University of Sydney and North Coast Cancer Institute, Lismore, NSW 2480, Australia

<sup>12</sup>Co-first author

\*Correspondence: rob.ramsay@petermac.org

<http://dx.doi.org/10.1016/j.celrep.2014.10.059>

This is an open access article under the CC BY-NC-ND license (<http://creativecommons.org/licenses/by-nc-nd/3.0/>).

## SUMMARY

**Loss of heterozygosity (LOH) of the adenomatous polyposis coli (APC) gene triggers a series of molecular events leading to intestinal adenomagenesis. Haploinsufficiency of the cohesin Rad21 influences multiple initiating events in colorectal cancer (CRC). We identify Rad21 as a gatekeeper of LOH and a  $\beta$ -catenin target gene and provide evidence that Wnt pathway activation drives RAD21 expression in human CRC. Genome-wide analyses identified Rad21 as a key transcriptional regulator of critical CRC genes and long interspersed element (LINE-1 or L1) retrotransposons. Elevated RAD21 expression tracks with reactivation of L1 expression in human sporadic CRC, implicating cohesin-mediated L1 expression in global genomic instability and gene dysregulation in cancer.**

## INTRODUCTION

Molecular pathways leading to colorectal carcinoma (CRC) are among the best defined of all cancers. Adenomatous polyposis coli (APC) gene mutations occur in most CRCs. Patients with familial polyposis (FAP) carry a heterozygous mutation in the APC gene (Cottrell et al., 1992), and loss of the second normal APC allele (loss of heterozygosity [LOH]) is necessary for colon polyp formation (Spirio et al., 1998). APC<sup>WT</sup> LOH is also a critical and early event in sporadic CRC (Clevers and Nusse, 2012; Cottrell et al., 1992). Mutant APC alleles mostly encode truncated proteins with compromised ability to regulate  $\beta$ -catenin degrada-

tion, allowing its nuclear translocation activating the canonical signaling pathway (Clevers and Nusse, 2012). APC truncation also compromises cytokinesis and chromosome segregation (Caldwell et al., 2007; Dikovskaya et al., 2007).

A central feature in most CRCs is chromosomal instability (CIN). Common mutations in CIN genes were recently identified in CRC (Barber et al., 2008). Strikingly, four of the five genes encode proteins essential for sister chromatid cohesion (SCC) (Nasmyth, 2001), suggesting that defects in SCC may underpin CIN. Indeed, small interfering RNA (siRNA) knockdown of SCC genes do show increased CIN (Barber et al., 2008).

SCC maintains physical connection between sister chromatids, ensuring balanced bipolar separation of chromatids in cell division (Nasmyth, 2001). SCC is also essential for homologous recombination (HR)-dependent repair of DNA breaks (Jessberger, 2009) and regulation of gene expression (Dorsett, 2011). SCC is orchestrated by the cohesin complex consisting of four subunits: Smc1, Smc3, Rad21/Scc1, and Scc3 (Nasmyth, 2001). Three of these subunits form a triangular or ring-shaped structural backbone, while the fourth subunit, Scc3, binds the complex through Rad21, which serves as the bridging protein linking the other three subunits (Haering et al., 2008).

We have been investigating Rad21/RAD21 in mouse gastrointestinal (GI) and human cancers (McKay et al., 1996; Xu et al., 2010, 2011b; Yan et al., 2012). Unlike other cohesins, RAD21 dysregulation rather than mutations is common in epithelial cancers, including CRC (Barber et al., 2008; Deb et al., 2014; Xu et al., 2011a). Elevated RAD21 expression is associated with poor cancer prognosis (Deb et al., 2014; Xu et al., 2010, 2011b; Yan et al., 2012), while Rad21 haploinsufficiency leads to defective response to radiation-induced damage, increased CIN, and HR deficiency (Xu et al., 2010).

Despite the emerging importance of cohesin in cancer biology, how cohesin dysfunction contributes to carcinogenesis remains elusive (Xu et al., 2011a). Here, we report a comprehensive study of Rad21's role in GI carcinogenesis in mouse models and primary human cancers. Using the *ApcMin* mouse, a well-characterized model of FAP (Moser et al., 1992), we elucidate multiple roles of Rad21 in mediating early molecular events leading to adenoma formation.

## RESULTS

### Ex Vivo *Apc<sup>WT</sup>* LOH in Organoids Is DNA Damage Inducible

As *Apc<sup>WT</sup>* allelic LOH is thought to be the key early event in adenomagenesis, we asked if this event could be detected prior to the formation of any microscopically identifiable lesions and, furthermore, if this could be modulated in vitro. We developed an assay to detect *Apc<sup>WT</sup>* LOH using ex vivo cultured organoids from mouse small intestinal (SI) crypts (Figure 1A). *Apc<sup>Min/+</sup>* organoids were morphologically indistinguishable from those of wild-type (WT). Occasional cyst-like colonies ("de novo adenomas") were observed. These became more frequent when primary organoids were replated (Figure 1A). Cyst-like organoids phenocopied cultures established directly from adenomas.

LOH was determined in individual organoids using a restriction fragment length polymorphism (RFLP) assay. Individual organoids generate multiple crypt-like projections (Figure 1A), thus containing a population of mixed clones. Accordingly, we set parameters for measuring LOH: a Min/WT allelic ratio of <1.2 as no LOH, while LOH includes those in transition (Min/WT > 1.2) and those with completed LOH (no detectable or negligible WT allele; Figure S1A). Analysis revealed that a significant proportion (88%) of organoids were in transition, whereas only 0.6% organoids had completed LOH (Figure 1B). Remarkably, 85% of cyst-like organoids had completed LOH (Figures 1B and S1B). Coincident with the complete loss of the WT allele, full-length Apc protein was undetectable in cyst-like organoids (Figure S1C). Immunohistochemistry (IHC) further confirmed aberrant β-catenin subcellular localization, as a result of *Apc<sup>WT</sup>* LOH, in primary organoids and in cyst-like organoids (Figure S1D). No statistical difference in LOH in organoids established from different regions of SI existed (Figure S1E).

Since *Apc<sup>WT</sup>* LOH had been shown to be HR dependent (Hagis and Dove, 2003), we predicted that *Apc<sup>WT</sup>* LOH is induced by DNA damage. We treated *Apc<sup>Min/+</sup>* organoids with hydrogen peroxide ( $H_2O_2$ ).  $H_2O_2$ , a byproduct of endogenous oxidative metabolism, generates free radicals and oxygen species that induce DNA damage, including DNA double-strand breaks (DSBs) that are preferentially repaired by HR-dependent DNA repair. DSBs marked by the presence of γH2AX foci were clearly evident in organoids following  $H_2O_2$  treatment (Figure 1C). *Apc<sup>WT</sup>* LOH was detected in 100% organoids, a significant increase above untreated (Figure 1B; Table S1).

### Extensive CIN Is Evident following *Apc<sup>WT</sup>* LOH

We next investigated the status of CIN in the context of *Apc<sup>WT</sup>* LOH. Epithelial cells of SI primary organoids mostly maintained normal ploidy (>85% diploid), with no statistical differences be-

tween WT and *Apc<sup>Min/+</sup>* cells (Figure 1D; Table S2). However in cyst-like secondary organoids and in cell cultures established from *Apc<sup>Min/+</sup>* adenomas, aneuploidy (predominantly hypoploidy) was observed in ~65%–67% of cells (Figure 1D; Table S2). *Apc<sup>Min/+</sup>* mouse embryonic fibroblasts (MEFs) exhibited a significantly higher frequency of aneuploidy (Figure 1D; Table S2) and abnormal mitotic cells, with multipolar spindles being the most frequent form (Figures 1E and 1F).

### *Rad21* Haploinsufficiency Delays Adenomagenesis in *Apc<sup>Min/+</sup>* Mice

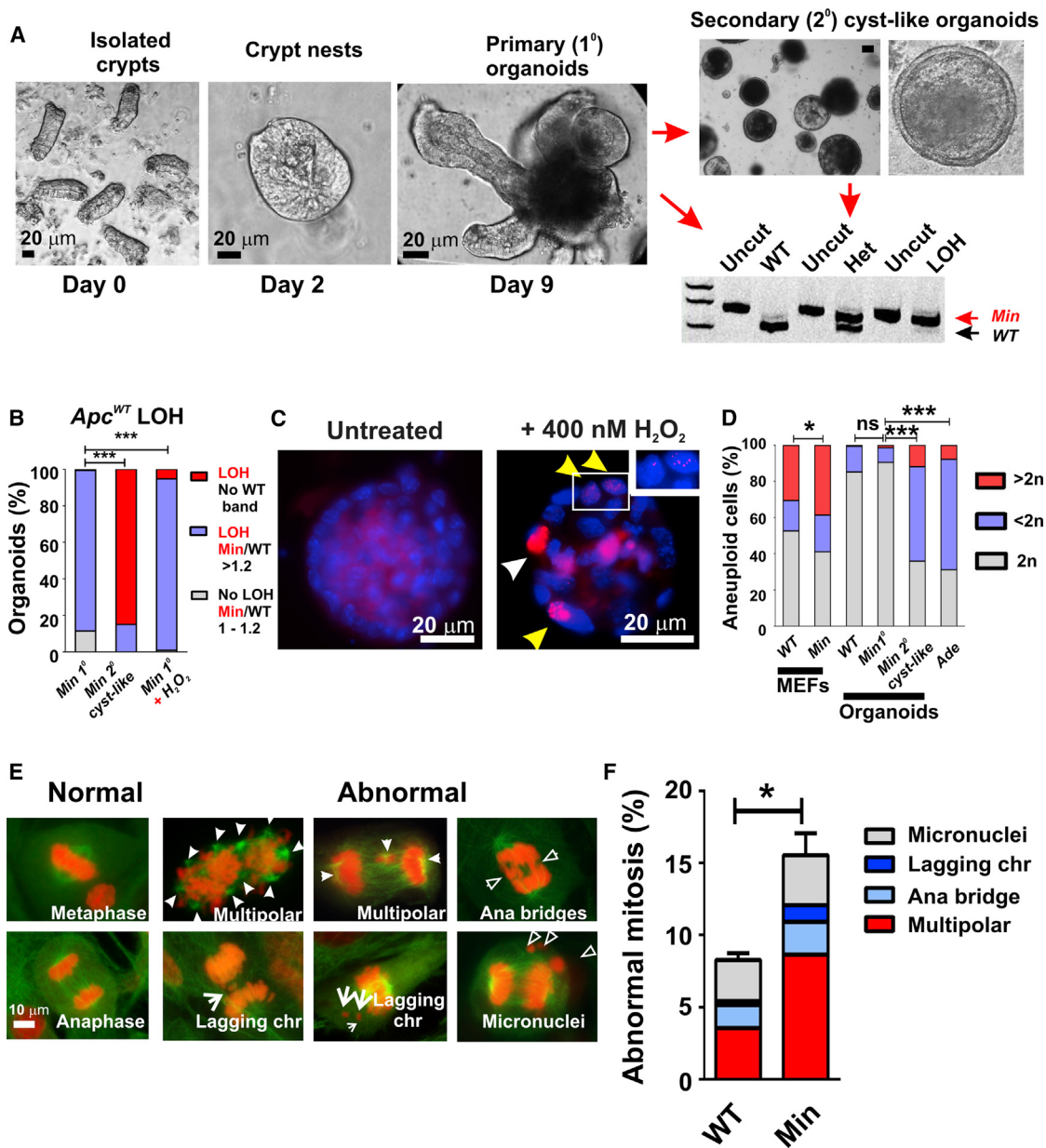
Given that cohesin is required for both HR and accurate chromosome segregation, the two processes implicated in the initiation of adenomagenesis, we set out to address any such role of cohesin by evaluating mutant mice lacking one *Rad21* allele. *Rad21* expression was detected predominantly in nuclei of multiple cell types in GI, including epithelial cells of both crypts and villi along the entire SI as well as the colonic crypts (Figure S2A). The most intense signal was observed in Paneth cells, which support the leucine-rich repeat-containing G protein-coupled receptor 5 (Lgr5)-positive intestinal stem cells (ISCs; Figure S2B). *Rad21* expression showed no regional differences in SI (Figure S2C) but was significantly reduced in both small and large intestinal crypts of *Rad21<sup>+/-</sup>* mice (Figure S2D).

When compared with *Apc<sup>Min/+</sup>* mice, double-mutant *Apc<sup>Min/+</sup>:Rad21<sup>+/-</sup>* mice showed statistically increased survival (Figure 2B). The presence of multiple adenomas, predominantly in the SI and, to lesser extent, in the colon or both, was confirmed in a subset of sick mice (Figure 2B). *Apc<sup>Min/+</sup>:Rad21<sup>+/-</sup>* exhibited a significant reduction in tumor incidence (20/24 [83.3%] compared to 43/43 [100%] for *Apc<sup>Min/+</sup>* mice; Table S3). Adenoma numbers were not significantly different at different GI sites between genotypes (Figure S2E). Further, two out of six (33.4%) *Apc<sup>Min/+</sup>:Rad21<sup>+/-</sup>* animals developed adenomas at a young age (<100 days), a significant decrease compared to seven out of seven (100%) *Apc<sup>Min/+</sup>* mice (Table S3). The number and size of SI adenomas was also significantly reduced in young *Apc<sup>Min/+</sup>:Rad21<sup>+/-</sup>* mice (Figures 2C and S2F). These results indicate a delay in SI adenoma formation on a *Rad21<sup>+/-</sup>* genetic background.

### *Rad21* Haploinsufficiency Impedes *Apc<sup>WT</sup>* LOH and Resolves Aneuploidy in *Apc<sup>Min/+</sup>* Cells

Organoids from *Apc<sup>Min/+</sup>:Rad21<sup>+/-</sup>* mice showed a significant reduction in the frequency of *Apc<sup>WT</sup>* LOH (Figure 2D). Adenomas harvested from mice showed LOH in 37 out of 39 (94.5%) *Apc<sup>Min/+</sup>* and 10 out of 11 (90%) in *Apc<sup>Min/+</sup>:Rad21<sup>+/-</sup>* mice (Figure 2D). In azoxymethane (AOM)-induced adenomas, *Apc<sup>WT</sup>* LOH was significantly reduced from 68.8% (22/32) to 34.3% (12/35) on a *Rad21<sup>+/-</sup>* background (Figure 2D). Since the propensity for *Apc<sup>WT</sup>* LOH has been found to be usurped by other mechanisms (Møller-Larsen et al., 2004), the reduction in *Apc<sup>WT</sup>* LOH in AOM-induced adenomas on a *Rad21<sup>+/-</sup>* background may be due to a deficiency in the pathways, such as HR, by which LOH arises.

To investigate whether the HR capability of intestinal cells was altered on a *Rad21<sup>+/-</sup>* background, we evaluated the frequency of sister chromatid exchange (SCE), a surrogate assay for HR, in primary intestinal organoids following treatment with mitomycin

**Figure 1. Ex Vivo Apc<sup>WT</sup> LOH Is Accelerated by DNA Damage and Associated with Extensive CIN**

(A) Individual organoid-based RFLP assay used for the evaluation of the Apc<sup>WT</sup> LOH. HindIII digestion of PCR products produces two fragments corresponding to the WT and Min alleles.

(B) Percentage of Apc<sup>WT</sup> LOH in organoids. No LOH, Apc<sup>WT</sup> to Apc<sup>Min</sup> allelic ratio <1.2; LOH, ratio >1.2 and no WT band.

(C) γH2X foci (yellow arrowheads) and extensive DNA fragmentation (white arrowhead) in Apc<sup>Min/+</sup> organoids treated with H<sub>2</sub>O<sub>2</sub>. Inset: enlarged view of the boxed region.

(D) Percentage of diploid (2n), hypoploid (<2n), or hyperploid (>2n) cells in MEFs, primary and secondary cyst-like organoids, and cell cultures established from Apc<sup>Min/+</sup> adenomas (Ade).

(E) Representative MEF cells showing abnormal mitoses: multipolar spindles (arrowheads), lagging chromosomes (arrows), anaphase bridges (open arrows), and micronuclei (open arrowheads). Mitotic spindles were revealed by α-tubulin staining (green) and DNA by propidium iodide (red). Ana, anaphase.

(F) Percentage of abnormal mitoses in MEFs. Total mitotic cells scored: WT n = 399; Min: Apc<sup>Min/+</sup> n = 388.

Data represent mean ± SEM. \*p < 0.05; \*\*p < 0.01; \*\*\*p < 0.001; ns, not significant. See also Figure S1 and Tables S1 and S2.

C (MMC), DNA damage from which is repaired preferentially by HR-dependent mechanisms (Sonoda et al., 1999). WT mouse intestinal cells had an average of 4.6 SCEs/metaphase. SCEs were

reduced to an average of 3.8/metaphase in the double-mutant Apc<sup>Min/+</sup>:Rad21<sup>+/−</sup> organoids; a statistically significant reduction compared to Apc<sup>Min/+</sup> organoids (Figure 2E).

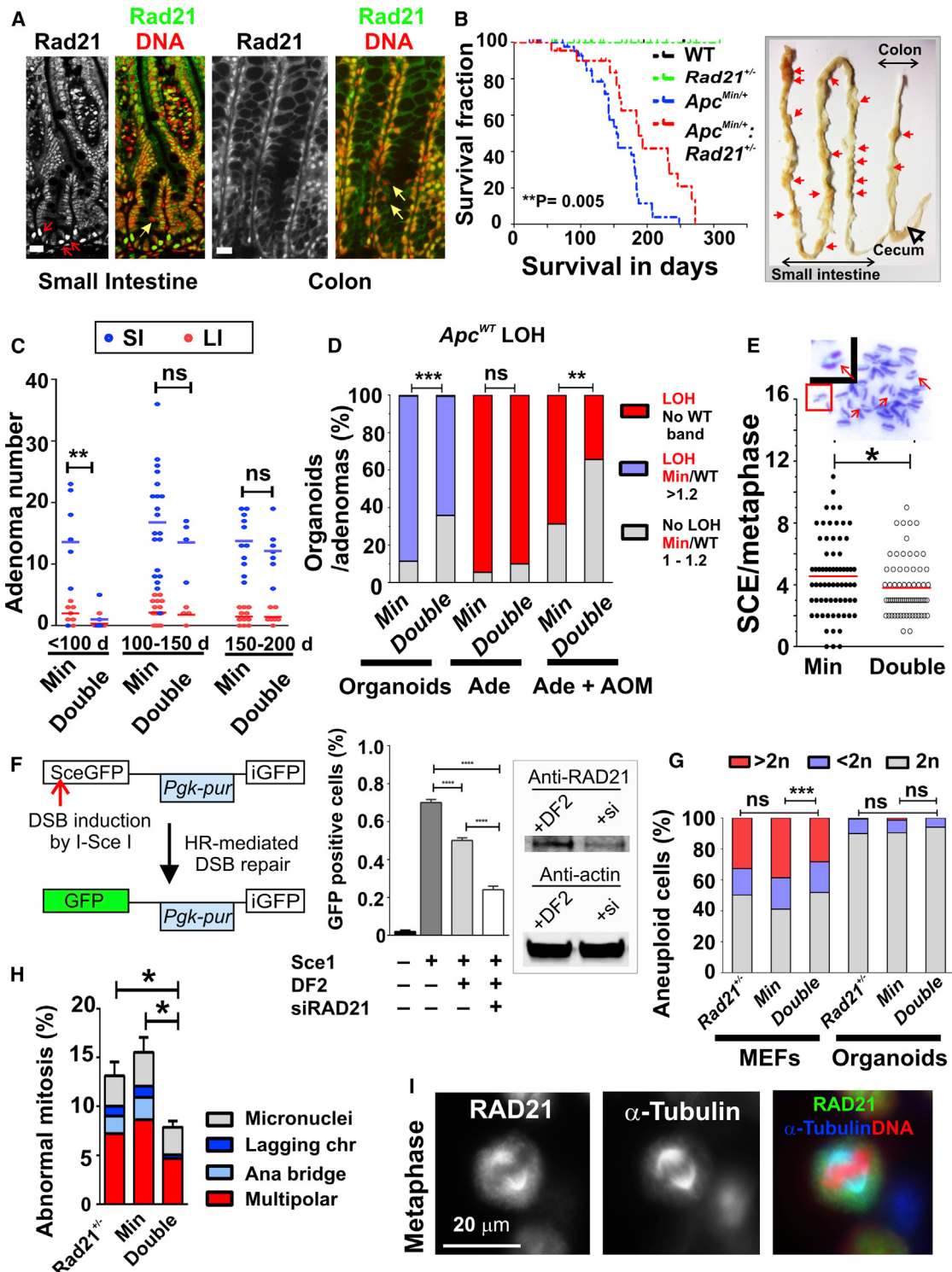


**Figure 2. *Rad21* Haploinsufficiency Affects Survival, Adenoma Formation, *Apc*<sup>WT</sup> LOH, and CIN**

(A) Immunofluorescence (IF) of Rad21 localization in small intestine (SI) and large intestine (LI, colon). Monochrome images in black and white. Rad21 (green) and nuclear DNA (red) colocalization (yellow). Paneth cells, red arrows; mitotic cells, yellow arrows. Scale bars represent 20  $\mu\text{m}$ .

(B) Kaplan-Meier survival plot of animals. WT n = 25;  $\text{Rad}21^{+/+}$  n = 32;  $\text{Apc}^{\text{Min}/+}$  n = 51;  $\text{Apc}^{\text{Min}/+} \cdot \text{Rad}21^{-/-}$  n = 30. Right: multiple adenomas throughout the intestines (red arrows).

(C) Adenoma incidence at different murine ages.

(legend continued on next page)

To ascertain the effect of Rad21 deficiency on HR, we employed a GFP-reporter assay, which allows for a more direct measure of HR in vitro (Pierce et al., 1999). We generated HCT116 cell clones with stable integration of an HR substrate containing a mutated GFP (SceGFP) and an internal region of GFP (iGFP; Figure 2F). The transient expression of I-Sce I endonuclease induces a DSB site that is subsequently repaired via HR using iGFP as a template, producing GFP+ cells (Figure 2F). siRNA-mediated *RAD21* depletion resulted in a significant reduction in the frequency of GFP+ cells (Figure 2F), demonstrating an essential role for RAD21 in mediating HR.

The effect of combined *Rad21* heterozygous loss and *Apc*<sup>Min</sup> mutations on CIN was investigated in MEFs and primary epithelial organoids. *Apc*<sup>Min/+</sup>:*Rad21*<sup>+/-</sup> double mutants showed a lower percentage of aneuploidy in MEFs (Figure 2G cf. Figure 1E; Table S2), but not in primary organoid epithelial cells (Figure 2G; Table S2). *Apc*<sup>Min/+</sup>:*Rad21*<sup>+/-</sup> double-mutant MEFs appeared to have restored mitotic integrity to a level comparable to WT, with a reduction in multipolar cells (Figure 2H). These data suggested a possible interplay between Rad21 and Apc at the mitotic spindle. RAD21 was indeed detected at mitotic spindles, colocalizing with  $\alpha$ -tubulin in CRC cells (Figure 2I).

#### ***Rad21* Heterozygous Deletion Reduces *Lgr5* Expression in ISCs and Compromises ISC Self-Renewal following *Apc*<sup>WT</sup> LOH**

ISC plays a critical role in adenomagenesis (Barker et al., 2009). We investigated the effect of *Rad21* heterozygous loss on ISC gene expression and activity. The ISC population is enriched for high aldehyde dehydrogenase (ALDH) activity, a functional marker of stem/progenitor cells (Moreb, 2008). Among known ISC markers, the expression of *Lgr5* was significantly reduced in *Rad21*<sup>+/-</sup> ISCs, while the expression of *Bmi1*, *Tert* (telomerase reverse transcriptase) and *Sox9* (SRY box9) was not affected (Figure 3A).

To assess the effect of *Rad21* heterozygous deletion on ISC self-renewal, the frequency of organoids formed from single cells of primary SI organoids was used as a readout (Sato et al., 2009). No statistically significant difference in the efficiency of organoid formation was found among the four genotypes (Figure 3B). When the self-renewal of cyst-like organoids was assessed in view of our finding that the majority of cyst-like organoids had completely lost the *Apc* WT allele (Figure 1B), *Apc*<sup>Min/+</sup>:*Rad21*<sup>+/-</sup> cyst-like organoids exhibited a marked reduction in the efficiency of organoid formation (Figure 3C).

#### ***Rad21* Heterozygous Loss Alters Gene Expression on a Global Scale**

To identify genes whose expression is affected by *Rad21* haploinsufficiency, we compared the gene expression profiles of crypt epithelial cells and adenomas from *Apc*<sup>Min/+</sup> and *Apc*<sup>Min/+</sup>:*Rad21*<sup>+/-</sup> double-mutant mice by RNA sequencing (RNA-seq). Gene expression profiles of crypts from *Apc*<sup>Min/+</sup> and *Apc*<sup>Min/+</sup>:*Rad21*<sup>+/-</sup> mice are likely to represent the transition from normal to the early stage of adenomagenesis, given that there were >50% mapped sequence reads corresponding to the mutant allele of the *Apc* gene (Figure S3A). Hierarchical clustering identified genes associated with *Rad21* heterozygosity (Figure 3D). This was more evident in crypts than adenomas. We reasoned that the effect of *Rad21* heterozygous loss on gene expression may have been attenuated by the upregulation of *Rad21* expression in adenomas. Quantitative RT-PCR (qRT-PCR) confirmed that the steady-state level of *Rad21* transcripts was not significantly altered in *Apc*<sup>Min/+</sup>:*Rad21*<sup>+/-</sup> adenomas compared to *Apc*<sup>Min/+</sup> adenomas (Figure 3E). By contrast, the level of *Rad21* transcripts was significantly reduced in crypts of *Apc*<sup>Min/+</sup>:*Rad21*<sup>+/-</sup> double mutants (Figure 3E). Interrogation of gene expression profiles of crypts between *Apc*<sup>Min/+</sup> single and *Apc*<sup>Min/+</sup>:*Rad21*<sup>+/-</sup> double mutants identified 3,869 genes that showed significantly altered expression on a *Rad21*<sup>+/-</sup> background, of which 55 genes showed changes greater than 4-fold (Table S4). qRT-PCR verified the changes in the expression of several affected candidate genes including upregulated genes *Akap12* (A kinase anchoring protein 12) and homeobox-containing transcription factor *Hoxb9*, and downregulated genes mannan-binding lectin *Mbl2*, *Sparc 1* (secreted protein, acidic, cysteine-rich glycoprotein), and a member of cytochrome P450 (CYP) mono-oxygenases, *Cyp1a2* (Figure 3F). Genes with altered expression between *Apc*<sup>Min/+</sup> and *Apc*<sup>Min/+</sup>:*Rad21*<sup>+/-</sup> crypts were significantly enriched for functions such as mitotic checkpoint, chromosome condensation, DNA damage checkpoint, and apoptosis (Figure 3G). Comparison of gene expression profiles between adenomas from *Apc*<sup>Min/+</sup> single- and *Apc*<sup>Min/+</sup>:*Rad21*<sup>+/-</sup> double-mutant mice showed relatively modest changes. Among 601 genes with significantly altered expression, only 63 genes showed changes greater than 2-fold (Table S5). The altered expression of genes such as *Abpa* (amylase-binding protein A), *DNase 1* (deoxyribonuclease 1), and *Mcpt9* (mast cell protease 9) was validated by qRT-PCR (Figure 3H).

*Rad21* heterozygosity also affected the expression of Wnt target genes, with genes such as *Axin2*, *gastrin*, and *Wnt4* being significantly downregulated but not for genes such as *c-Myc* and

(D) Percentage of *Apc*<sup>WT</sup> LOH in organoids, adenomas (Ade), and AOM-induced adenomas.

(E) MMC-induced SCEs in primary intestinal epithelial cells from organoid cultures. Insert: a representative metaphase chromosome spread showing SCE (arrows) with an enlarged view of SCE (box).

(F) DR-GFP recombination assay in HCT116 cells. Left: diagrammatic representation of the assay. Middle: percentage of GFP-positive cells in siRNA treated and control cells. DF2, DharmaFECT 2 transfection reagent. Right: western blot validation of RAD21 KD; actin, loading control.

(G) The percentage of diploid (2n), hypoploid (<2n), or hyperploid (>2n) cells in MEFs and primary organoids.

(H) Percentage of abnormal mitoses in MEFs. Total mitotic cells scored: *Rad21*<sup>+/-</sup> n = 280; *Apc*<sup>Min/+</sup> n = 388; *Rad21*<sup>+/-</sup>:*Apc*<sup>Min/+</sup> double mutant n = 395; Chr, chromosome(s); Ana, anaphase.

(I) IF of LIM1215 colon cancer cells. RAD21 (green) and  $\alpha$ -tubulin (blue) colocalization (light blue) on the mitotic spindle in the merged image; DNA (red). Min: *Apc*<sup>Min/+</sup>; Double, *Rad21*<sup>+/-</sup>:*Apc*<sup>Min/+</sup> double mutant.

Data represent mean  $\pm$  SEM. \*p < 0.05; \*\*p < 0.01; \*\*\*p < 0.001; ns, not significant. See also Figures S1 and S2 and Tables S1–S3.

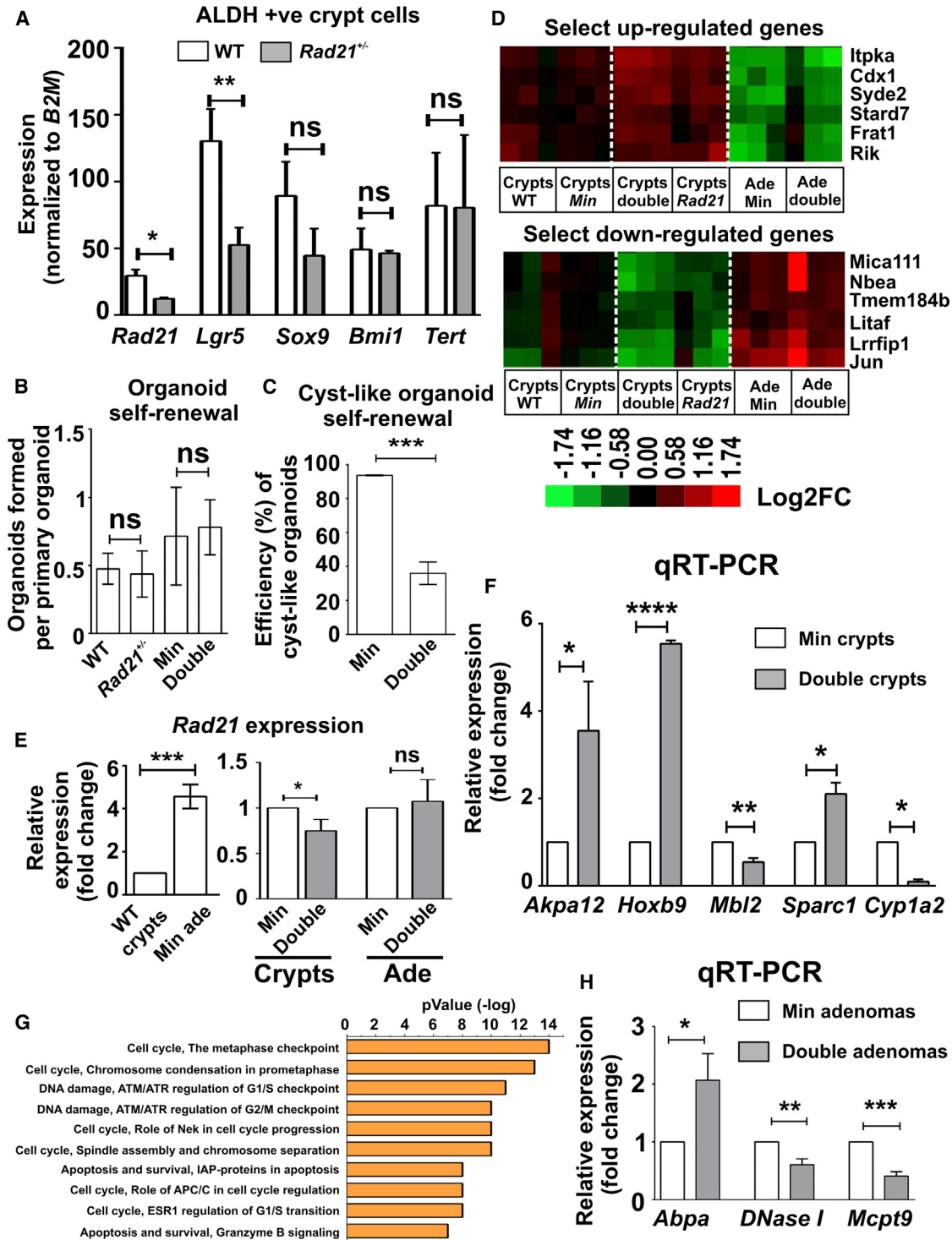


**Figure 3. The Effect of Rad21 Heterozygosity on Intestinal Stem Cell Gene Expression and Self-Renewal**

- (A) qRT-PCR of intestinal stem cell (ISC) marker gene expression in WT and *Rad21*<sup>+/−</sup> ALDH<sup>+</sup> cells. Expression was normalized to  $\beta2M$ . WT n = 3; *Rad21*<sup>+/−</sup> n = 4.
- (B) Organoid self-renewal assay for stem cell activity. WT n = 7; *Rad21*<sup>+/−</sup> n = 3; *Apc*<sup>Min/+</sup> n = 4; Double n = 4.
- (C) Cyst-like organoid self-renewal. *Apc*<sup>Min/+</sup> n = 3; Double n = 8.
- (D) Heatmaps of representative gene clusters showing selected up- (top) and downregulated (bottom) genes associated with *Rad21* heterozygosity. Log<sub>2</sub>FC, log<sub>2</sub> fold change.
- (E) qRT-PCR of *Rad21* expression in SI crypts and adenomas. Right: WT n = 4; *Apc*<sup>Min/+</sup> adenomas n = 7. Left: *Apc*<sup>Min/+</sup> crypts n = 6; Double crypts n = 7, *Apc*<sup>Min/+</sup> adenomas n = 4; Double adenomas n = 4.

(legend continued on next page)

*Wnt3* (Figures S3B and S3C). Hierarchical analysis for an expanded list of known Wnt/β-catenin target genes identified clusters that are unique to *Apc*<sup>Min/+</sup>:*Rad21*<sup>+/-</sup> double-mutant crypts and, furthermore, revealed that the Wnt gene expression profile of double-mutant crypts are more closely related to WT than *Apc*<sup>Min/+</sup> crypts (Figure S3D). The analysis clustered *Apc*<sup>Min/+</sup>:*Rad21*<sup>+/-</sup> adenomas with *Apc*<sup>Min/+</sup> adenomas (Figure S3D).

### Elevated Rad21 Expression in Adenomagenesis Is Uncoupled from Proliferation

We performed immunostaining to determine when and where elevated Rad21 expression occurs during adenomagenesis in both *Apc*<sup>Min/+</sup> mice and human sporadic CRCs. Elevated but heterogeneous Rad21 staining was evident in cyst-like organoids, aberrant crypt foci (ACF), and adenomas of *Apc*<sup>Min/+</sup> mice (Figure 4A). RAD21 expression was elevated in five out of ten human CRC cell lines examined compared to the human embryonic kidney 293 (HEK293) cell line (Figure 4B). Immunostaining confirmed that RAD21 is predominantly nuclear (Figure 4C), as seen in other cancer cells (Xu et al., 2004).

To examine the association of RAD21 expression with proliferation, we performed coimmunostaining of RAD21 in normal colon with a proliferation marker Ki-67, since human colon, not SI, is the primary site of GI cancer. RAD21 was detected in ~80% of crypt epithelial cells (Figures 4D and 4E). At the bottom and middle proliferative regions of crypts, approximately one-third of RAD21+ cells colocalized with Ki-67, whereas at the upper region, the majority of cells were positive only for RAD21 (Figures 4D and 4E). In adenomas, RAD21 staining was observed in nearly all cells (Figures 4D and 4E). There was a statistically significant increase in RAD21/Ki-67 double-positive cells ( $28.2\% \pm 2.4\%$ ) compared to normal crypts ( $19.9\% \pm 1.3\%$ ;  $p = 0.0038$ ) and, furthermore, unlike in normal crypts, double-positive cells were observed along the entire length of crypts (Figures 4D and 4E). RAD21 and Ki-67 staining was similar in adenocarcinomas (Figure 4E). A similar pattern of Rad21/Ki-67 staining was observed in *Apc*<sup>Min/+</sup> mouse adenomas (Figure S4A). Rad21 staining in mouse adenomas appeared to be more heterogeneous compared to human polyps and CRC, possibly since mouse adenomas are generally early stage.

To directly assess the effect of elevated RAD21 expression on cell proliferation and cell-cycle progression, we overexpressed RAD21 in SW480 cells (Figure S4B). No difference in proliferation and cell-cycle progression was observed between RAD21-over-expressing and control cells (Figures 4F and S4C).

### RAD21 Is Regulated by β-Catenin Activation and Tracks with Aberrant β-Catenin Localization in Adenomas

Elevated Rad21 expression appeared to coincide with the activation of the Wnt/β-catenin pathway, as indicated by the aberrant subcellular (nuclear or loss of membrane) location of β-catenin (Figure 5A). We thus tested whether *Rad21* was a

direct β-catenin transcriptional target gene. Cotransfection of the *Rad21*-promoter-chloramphenicol acetyl-transferase (CAT) reporter with increasing activated (Δ89)-β-catenin levels showed the induction of the CAT reporter in a dose-dependent manner (Figure 5B). An examination of the 4 kb 5' upstream of the *Rad21* proximal promoter identified seven putative high-affinity binding sites for Tcf7L2/Tcf4 (T cell binding factor), which combines with β-catenin to activate the canonical Wnt signaling. These putative motifs are located in two clusters: one at the proximal region (-200 to -500 bp) and the other within the distal region of -3,600 to -3,800 bp (Figure 5C). ChIP-qPCR confirmed an enrichment of β-catenin at these regions compared to a control region lacking the motifs (Figure 5C).

Consistent with our mouse data, elevated RAD21 expression was clearly evident in CRC and coincided with aberrant β-catenin localization (Figure 5D). Tissue microarrays (TMAs) assembled from two large independent CRC patient cohorts (total of 529 sporadic cases) were examined for RAD21 and β-catenin staining. CRC samples showed variable RAD21 protein staining, ranging from negligible to very strong (Figure 5E). The mean histoscore, a combination of the intensity and percentage of positive cells, of RAD21 is significantly higher in tumors with aberrant β-catenin localization compared to those with normal membranous localization (9.27 versus 7.88 [ $p = 0.004$ ] in the first cohort and 6.0 versus 5.2 [ $p = 0.04$ ] in the second cohort). In both cohorts, tumors exhibiting a high level of RAD21 expression (i.e., histoscore 12) were more frequent in aberrant β-catenin groups (Figure 5E; Table S6). This was particularly evident in cohort 1, with 40 out of 84 (47.6%) cases in the aberrant group compared to 30 out of 124 (24%) cases in the normal group (Figure 5E; Table S6). These data suggest that, as in the *Apc*<sup>min/+</sup> mouse model, RAD21 expression is upregulated by Wnt/β-catenin activation in human CRC.

To directly assess the effect of the Wnt activation on *RAD21* expression, we blocked the Wnt signaling by either enforced expression of a dominant-negative TCF4 (dnTCF4) gene or ectopically expression of the WT APC gene (Faux et al., 2004). RAD21 expression was significantly reduced in both cases (Figure 5F).

### Genome-wide Analysis Identifies Rad21 as a Key Regulator of CRC Genes

To identify genes that are directly regulated by Rad21, we performed genome-wide mapping of Rad21 binding sites with ChIP sequencing (ChIP-seq) (Johnson et al., 2007). This analysis identified high confidence Rad21-occupied regions corresponding to sites unique to, or shared between, normal SI crypts and in *Apc*<sup>Min/+</sup> adenomas (Figures 6A and 6B). Consistently, Rad21 binding sites were found at gene loci known to be associated with Rad21, as exemplified by the Hox (homeobox) gene family (Schaaf et al., 2013) (Figure S5A).

(F) qRT-PCR validation of gene expression changes in *Apc*<sup>Min/+</sup> crypts compared to double-mutant crypts. *Apc*<sup>Min/+</sup> crypts n = 3; Double crypts n = 3.

(G) Top ten pathways with gene expression altered by *Rad21* heterozygosity.

(H) qRT-PCR validation of gene expression changes in *Apc*<sup>Min/+</sup> and double-mutant adenomas. *Apc*<sup>Min/+</sup> adenomas n = 4; Double adenomas n = 4. Min: *Apc*<sup>Min/+</sup>; Double: *Rad21*<sup>+/-</sup>:*Apc*<sup>Min/+</sup> double mutant.

Data represent mean ± SEM. \* $p < 0.05$ ; \*\* $p < 0.01$ ; \*\*\* $p < 0.001$ ; \*\*\*\* $p < 0.0001$ ; ns, not significant. See also Figure S3 and Tables S4 and S5.

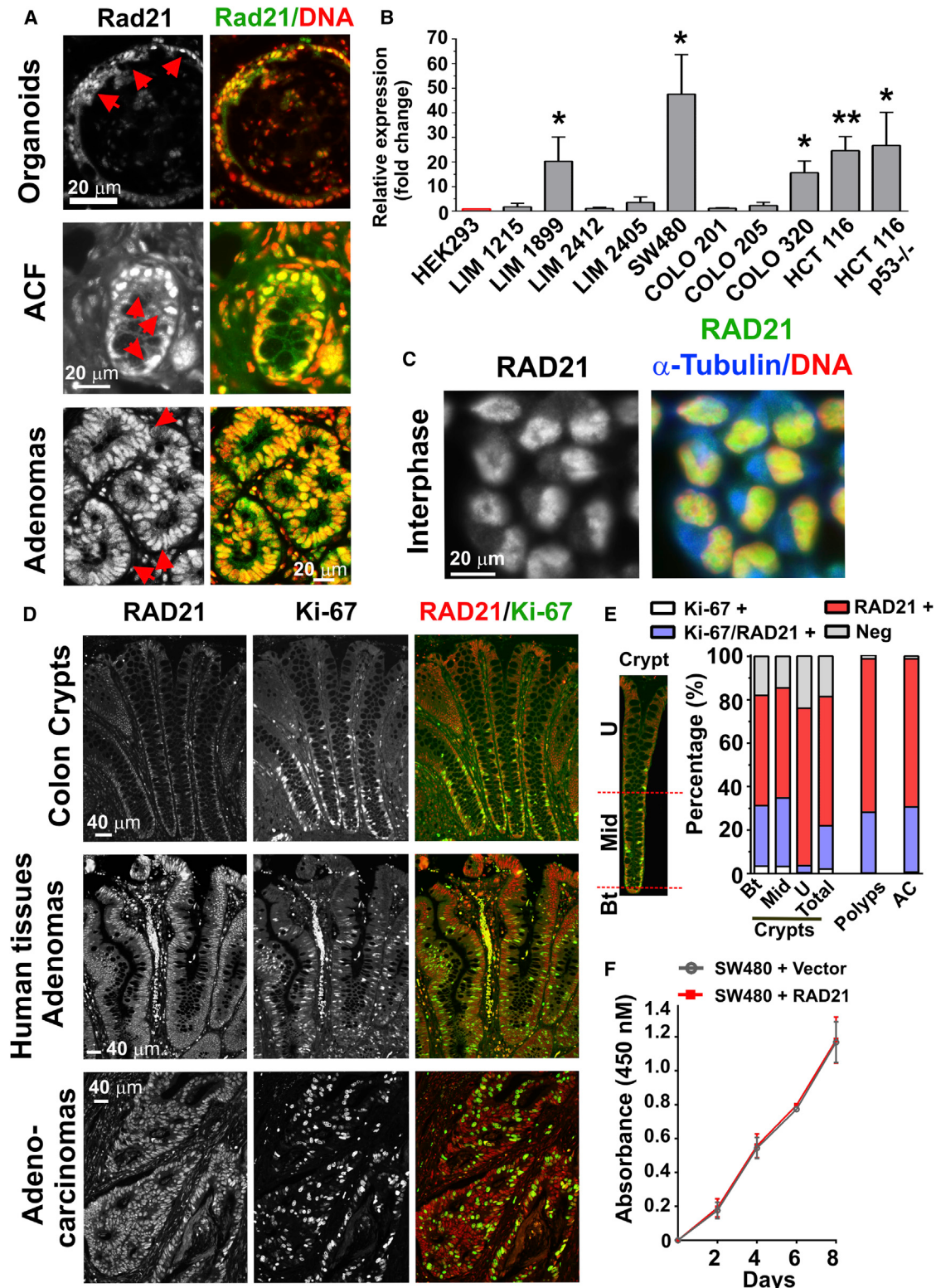


**Figure 4. Elevated Rad21 Expression in Mouse and Human Adenomagenesis Is Uncoupled from Proliferation**

(A) Immunofluorescence (IF) of Rad21 expression in *Apc<sup>Min/+</sup>* mouse organoids (top), ACF (middle), and adenomas (bottom). Monochrome images in black and white. Rad21 (green) and nuclear DNA (red) colocalization (yellow). Some nuclei (red arrows) showed a stronger Rad21 signal.

(legend continued on next page)

Rad21 was found to be enriched at the core promoters of known Wnt/β-catenin target genes in adenomas (eg, *Lgr5*; Figure 6C). The enrichment at the *Lgr5* promoter was independently confirmed by conventional ChIP (Figure 6C). The association of Rad21 with the promoters of two archetypical Wnt target genes, *c-Myc* and *Ccnd1*, was observed and confirmed by conventional ChIP (Figures S5B–S5D), noting that *c-Myc* is a known cohesin-regulated gene (Rhodes et al., 2010). Rad21 enrichment was also detected at the core promoter of cohesin gene *SMC3* (Figure 5D), suggesting that cohesin gene expression is autoregulated. As a negative control, we used conventional ChIP-qPCR to confirm that low Rad21 binding regions have nonsignificant Rad21 binding (Figure 6E). Collectively, these data suggest a coordinated transcriptional activation program that is regulated by Rad21 following *Apc*<sup>WT</sup> LOH.

### Rad21 Is Enriched in the Regulatory Regions L1 Retrotransposons

We scanned the Rad21-associated sequences for the presence of retrotransposons in ChIP-seq data sets. The analysis identified an enrichment of retrotransposons within high-confidence Rad21 binding regions in both crypt cells and *Apc*<sup>Min/+</sup> adenomas. These included short interspersed elements (SINEs), L1 and long terminal repeat (LTR) retrotransposons (Figure S6A).

Since L1 is the most abundant and the only retrotransposon capable of autonomous retrotransposition in the mammalian genome, we performed a more detailed analysis on L1. *L1* expression, which coincided with elevated *Rad21* expression, was detected in mouse adenomas (Figure S6B). Rad21 enrichment was found at the internal promoter within the L1 5' UTR tandem repeats (Figures 7A and 7B). Since the mouse L1 promoter is rich in CpG repeats, we used a methylation-sensitive enzyme (Hpall) digestion to determine whether Rad21 binding was influenced by the methylation status. Rad21-associated L1 promoter sequences amplified from both crypts and adenomas were fully digested by Hpall (Figures 7C and S6C), suggesting the absence of methylation. CTCF, a chromatin insulator and known Rad21 interactor, was also present at the L1 promoter sequences bound by Rad21 at representative loci corresponding to full-length L1 (Figure 7D).

### RAD21 Drives L1 Expression in Human CRC Cell Lines

An examination of a panel of ten human CRC cell lines revealed strongly correlated expression between *L1* and *RAD21* (Figure S6D). Likewise, the levels of L1 proteins, ORF1p and ORF2p, coincided with the abundance of RAD21 protein (Fig-

ure 7E). An apparent reduction in the levels of endogenous L1 protein was observed in LIM1215 cells following RAD21 knockdown (KD) by either siRNA or stable expression of small hairpin RNA (shRNA; Figure 7F), suggesting a close association between RAD21 and L1.

To directly assess the effect of RAD21 on L1 expression, we introduced a construct containing the human L1 5' UTR (promoter) driven GFP reporter gene under into HCT116 p53<sup>-/-</sup> cells. Stable GFP-expressing cells were obtained in cells with enforced RAD21 expression (Figures 7G and S6F). L1-GFP signal appeared stronger in cell doublets (mitotic cells; Figure 7G), correlating with RAD21 expression (Figure S6F). To ascertain that L1-GFP expression was RAD21 dependent, we assessed GFP expression following siRNA-mediated RAD21 KD. GFP signal was reduced or completely lost in some cells (Figure 7H). This phenotype was not observed in control cells transfected with mock siRNA (Figure 7H). Western blot further confirmed a reduction in GFP protein in siRNA KD cells compared to the mock-siRNA control (Figure 7H).

### L1 Expression Associates with Elevated RAD21 in Human Adenomas and CRC

To address the relationship between RAD21 and L1 expression in human CRC, we evaluated the expression of both proteins in adenocarcinomas. L1 was barely detectable in normal crypts but clearly evident in the cytoplasm and, in some cases, nuclei of adenocarcinomas (Figure 7I). Because the retrotransposition of L1 takes place in the nucleus, the presence of nuclear L1 is indicative of retrotransposon activities. Strong RAD21 staining was detected in cells that are positive for L1 staining (Figure 7I). Examination of L1 expression in TMAs consisted of 142 adenocarcinomas showed a statistically significant association between elevated RAD21 and L1 expression (Figure 7J). These data suggest that L1 activation is an early event in CRC development and that RAD21 is a probable regulator of L1 expression.

### DISCUSSION

The *Apc*<sup>Min/+</sup> mouse model affords the opportunity to investigate the earliest events in the development of CRC and it is remarkable how many of the requisite events are influenced by cohesin function. Here, we show that *Rad21* haploinsufficiency affects the initiating events of adenomagenesis in *Apc*<sup>Min/+</sup> mice. Further, we found that *Rad21* is a direct Wnt pathway target connecting the elevated expression of Rad21 with aberrant β-catenin localization. Finally, our genome-wide analysis revealed a key

(B) qRT-PCR of RAD21 expression in a panel of human CRC cell lines. Expression was normalized to the *PGK* gene and fold change calculated relative to HEK293. \*p < 0.05.

(C) IF of RAD21 in LIM1215 cells showing predominant nuclear localization in interphase cells.

(D) Co-IF of RAD21 and proliferation marker Ki-67 in human normal crypts (top), adenomas (middle), and adenocarcinomas (bottom). Monochrome images in black and white. RAD21 (red) and Ki-67 (green) colocalization (yellow) in merged images. Note the intense staining of both RAD21 and Ki-67 in lymphocytes located between dysplastic crypts (middle).

(E) Quantitation of data shown in (D). Left: a representative normal crypt showing the partitioning of three crypt compartments: bottom (Bt), middle (Mid), and upper (U). Data represent the mean of ten normal crypts (n = 2,184 nuclei), five polyps (n = 6,135 nuclei), and ten random microscopy fields (40×) of adenocarcinomas (n = 8,802 nuclei). AC, adenocarcinomas.

(F) Proliferation of the SW480 cell clone with stable enforced RAD21 expression compared to the vector control clone. Data represent mean ± SEM of three independent experiments.

See also Figure S4.

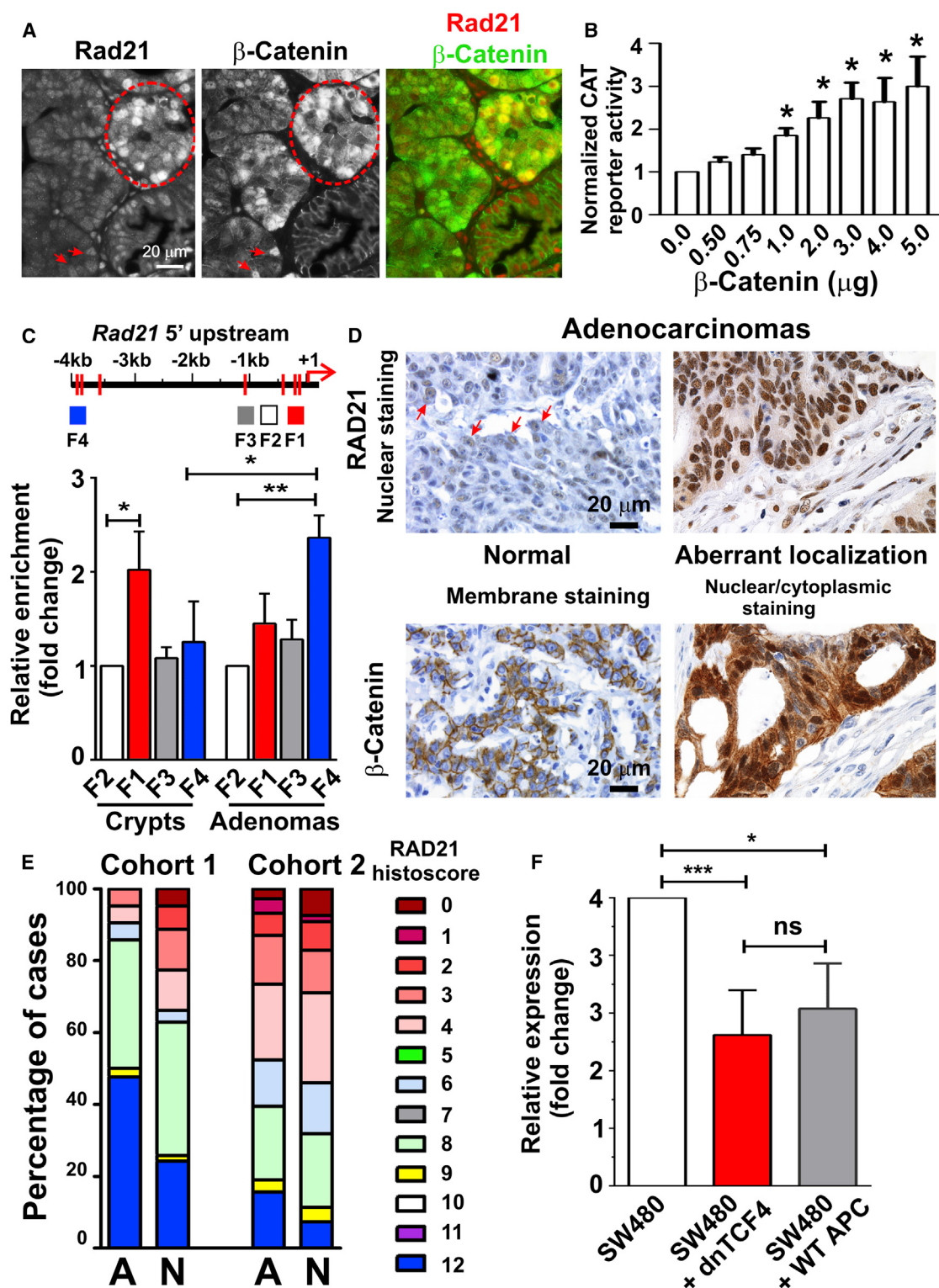


**Figure 5. RAD21 Expression Tracks with Aberrant β-Catenin Localization during Adenomagenesis and Is a Direct β-Catenin Target Gene**  
(A) Co-IF of Rad21 and β-catenin in *Apc*<sup>Min/+</sup> adenomas. Monochrome images in black and white. Rad21 (red) and β-catenin (green) colocalization in some regions (red circle and arrow). Note the apparent colocalization of aberrant nuclear β-catenin staining with enhanced Rad21 signal in some regions (red circle and arrow).  
(B) CAT reporter assay showing transactivation of the mouse *Rad21* promoter by increasing activated β-catenin. Data represent mean ± SEM of three independent experiments.

(legend continued on next page)

role for Rad21 in global gene transcription and particularly in the expression of L1 retrotransposons. Our study of human sporadic CRC recapitulated these findings, supporting a role for RAD21 in the initiation and progression of human CRC through multiple mechanisms.

#### **Rad21 Is a Key Mediator of *Apc*<sup>WT</sup> LOH**

*Apc*<sup>WT</sup> LOH is frequently observed in human FAP (Spiro et al., 1998) and sporadic CRC (Clevers and Nusse, 2012; Cottrell et al., 1992), leading to the suggestion that this is an initiating event in CRC. A number of mechanisms for the genesis of LOH have been proposed (Caldwell et al., 2007; Dikovskaya et al., 2007; Haigis and Dove, 2003; Moynahan and Jasin, 2010). These include gene conversion via HR (Haigis and Dove, 2003; Moynahan and Jasin, 2010) and whole-chromosome gain or loss due to mitotic defects (Caldwell et al., 2007; Dikovskaya et al., 2007). We demonstrated that *Apc*<sup>WT</sup> LOH can be accelerated in vitro through the induction of oxidative DNA damage. Our data suggest that DNA damage and, presumably, its subsequent repair contribute to *Apc*<sup>WT</sup> LOH, supporting a role for HR in mediating LOH.

Our study revealed that *Rad21* haploinsufficiency led to a significant reduction in *Apc*<sup>WT</sup> LOH, providing evidence that Rad21 is a critical factor in mediating this event. We suggest that Rad21 contributes to this event primarily through its role in HR. Our findings that *Rad21* haploinsufficiency led to a significant decrease in the frequency of SCEs and that siRNA KD of RAD21 impeded HR provide compelling evidence supporting a role for Rad21 in HR-mediated *Apc*<sup>WT</sup> LOH.

#### **Increased CIN Is Evident in De Novo Adenoma and Associated with *Apc*<sup>WT</sup> LOH**

Cell-based and intestinal crypt studies indicate that the first histologically discernible step toward CIN in *Apc* mutant cells involves mitotic spindle misorientation (Fleming et al., 2009) and subsequent tetraploidy (Caldwell et al., 2007; Dikovskaya et al., 2007). Although CIN tracks closely with LOH of the *Apc* gene, the interplay between these events is not well understood. Our results show that although chromosomal numerical aberrations of primary *Apc*<sup>Min/+</sup> MEFs were high and concordant with an abnormal, largely hyperploid complement, there is no evidence of increased CIN in *Apc*<sup>Min/+</sup> primary epithelial cells of organoids, even though LOH was present. There is, however, a marked increase in CIN in cyst-like organoids. Thus, the increase in CIN coincides with completed *Apc*<sup>WT</sup> LOH in these cells and that *Apc*<sup>WT</sup> LOH appears to precede CIN.

Our data further revealed that *Rad21* heterozygosity reduces CIN in *Apc*<sup>Min/+</sup> cells in MEFs and primary organoids. How

*Rad21* haploinsufficiency restores this abnormality is at present unclear. *Apc*<sup>Min/+</sup>:*Rad21*<sup>+/-</sup> mutant cells had a significant reduction in the multipolar type of abnormal mitoses implies a functional crosstalk between APC and RAD21 at mitotic spindles. Consistent with this notion, APC has been shown to be localized at the mitotic spindle apparatus (Fleming et al., 2009) and the *Apc*<sup>Min</sup> mutation impairs the spindle checkpoint through its interaction with Mad2 (Zhang et al., 2009). Likewise, we and others found that RAD21 and SMC1 are localized at mitotic spindles (Wong and Blobel, 2008). Furthermore, cohesin was shown to be recruited to the spindle poles by nuclear mitotic apparatus protein (NuMA) (Kong et al., 2009). We suggest that Rad21 deficiency may directly or indirectly antagonize this effect by restoring the spindle checkpoint, leading to the elimination of aberrant mitotic cells that would otherwise have given rise to aneuploid cells.

#### **Effects of Rad21 Overexpression Are Uncoupled from Proliferation**

Could the modulation of Rad21 expression and the myriad of consequences on adenomagenesis be due to a direct role of Rad21 in regulating proliferation? Biological data from analysis of Rad21 heterozygous GI crypt proliferation suggested that this was unlikely (Xu et al., 2010). Furthermore, we found non-concordance of Ki-67 and Rad21/RAD21 expression in mouse and human crypts, adenomas, and carcinomas. Enforced RAD21 expression did not affect proliferation and cell-cycle progression in SW480 cells. We thus conclude that Rad21 mediates its many effects by processes independent of proliferation.

Genes that regulate cell cycle were substantially affected in *Apc*<sup>Min/+</sup> crypts by *Rad21* haploinsufficiency in our RNA-seq analyses. This effect maybe an indirect consequence of *Rad21* deficiency, for example, delayed S phase progression (Guillou et al., 2010), impaired spindle assembly (Kong et al., 2009), or altered chromosome architecture (Zuin et al., 2014). Additionally, these changes in gene expression may reflect a global transcriptional change at the very early stages of adenomagenesis.

#### **Upregulation of Rad21 via Wnt/β-Catenin Activation Is an Early Event in CRC**

RAD21 upregulation occurs in approximately half of human CRCs (Deb et al., 2014). We found that elevated RAD21 expression occurs at the early stages of carcinogenesis. How *RAD21* expression is upregulated in CRC is unknown. *RAD21* upregulation was shown to be associated with gene amplification in high-grade breast cancer (Xu et al., 2011b) and with *c-Myc* gene amplification in CRC (Deb et al., 2014). Since the *RAD21* gene

(C) ChIP-qPCR showing the enrichment of β-catenin binding at the mouse *Rad21* 5' upstream regions (red, gray, and blue boxes) that contain high-affinity Tcf7L2/Tcf4 binding motifs (red bars) compared to a negative control region lacking the motif (F2, open box). Data represent mean ± SEM of three independent ChIP assays.

(D) Representative images of human CRC TMA showing weak (arrows, top left) and strong (top right) RAD21 nuclear staining and aberrant β-catenin localization. Adjacent sections were appraised for either membranous only (normal) or aberrant β-catenin staining.

(E) Correlation of normal β-catenin membrane or aberrant localization with RAD21 expression in two independent cohorts of human CRCs (cohort 1 n = 206; cohort 2 n = 323). RAD21 histoscore (0–12); A, aberrant localization; N, normal membrane staining.

(F) qRT-PCR of RAD21 expression in SW480 cells showing reduced RAD21 expression following either transient expression of dnTCF4 or the restoration of WT APC expression.

Data represent mean ± SEM of six independent transient transfections for dnTCF4 and three independent harvests of SW480+WT APC cells. \*p < 0.05; \*\*p < 0.01; \*\*\*p < 0.001. See also Figure S3 and Table S6.

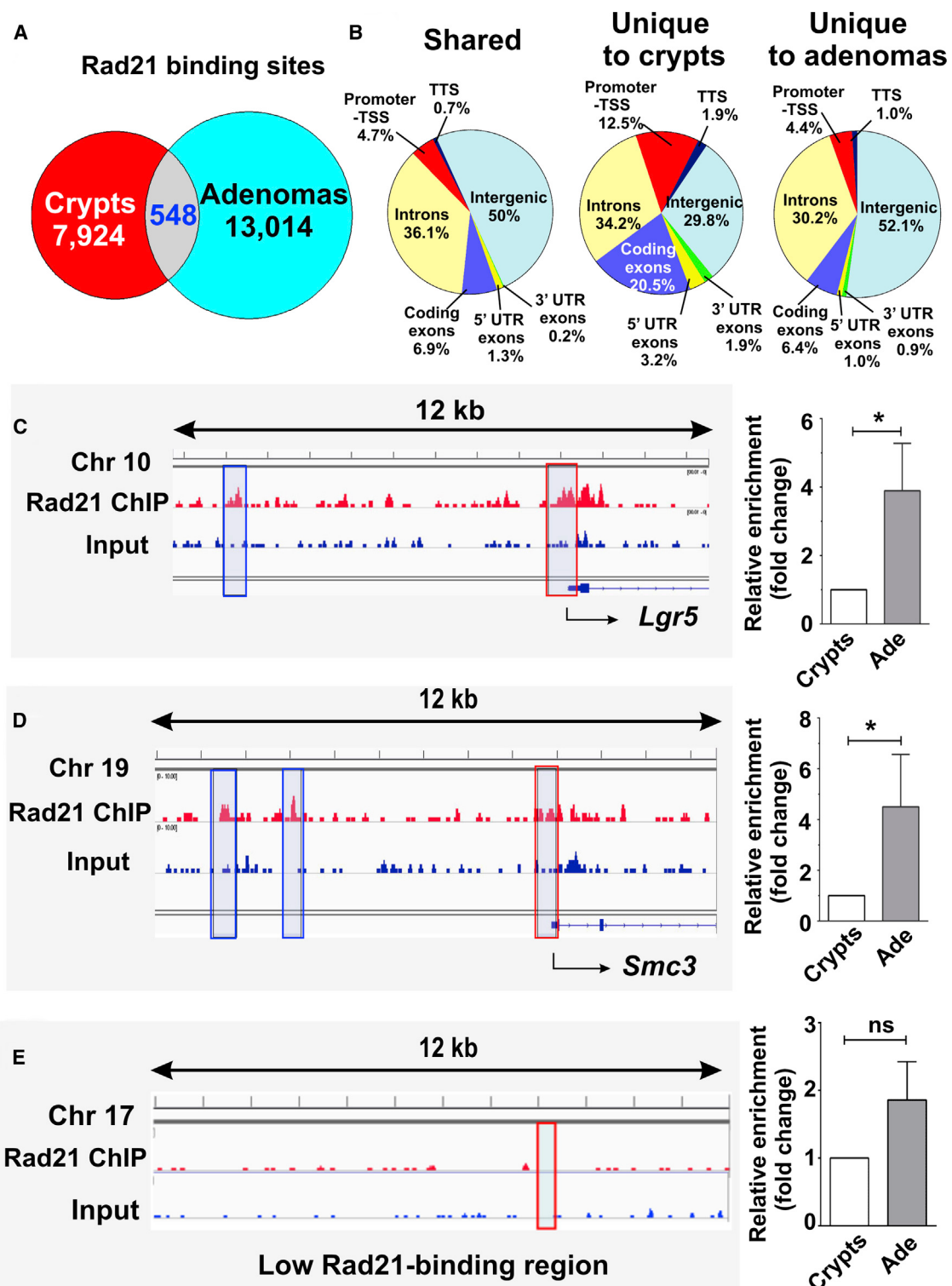


**Figure 6. Rad21 Binds to Key CRC Genes in *Apc*<sup>Min/+</sup> Adenomas**

(A) Venn diagram showing the distribution of unique and shared Rad21 binding sites.

(B) Pie charts showing the percentage of high-confidence Rad21 binding regions at gene transcriptional start sites (TSS), 5' or 3' UTR exons, coding exons, introns, and intergenic regions.

(legend continued on next page)

locates at 8q24, a region that encompasses *c-Myc* and commonly amplified in epithelial cancers, *RAD21* overexpression may simply be consequence gene amplification at 8q24.

Our data that elevated Rad21 expression associated with aberrant  $\beta$ -catenin subcellular location in intestinal tumors raise the further possibility that *Rad21* upregulation occurs through Wnt/ $\beta$ -catenin signaling.  $\beta$ -Catenin binds to the *Rad21* promoter and is capable of driving *Rad21-CAT* reporter expression. Furthermore, RAD21 expression in human CRC cells was directly modulated by Wnt/ $\beta$ -catenin activation, in that *RAD21* expression was found to be significantly reduced when Wnt/ $\beta$ -catenin signaling was blocked. Upregulation of *Rad21* expression via aberrant Wnt/ $\beta$ -catenin activation seems to be an early event in human CRC.

### **Rad21 Positively Regulates the Expression of GI Stem Cell and CRC Genes**

Our genome-wide analysis revealed the association of Rad21 with the core promoters/transcription start sites (TSSs) of approximately 5%–12% of genes, while the majority of Rad21 binding sites mapped to intergenic or intronic regions. This is consistent with the known role for cohesin in regulating transcription, either by direct interaction with Pol II transcriptional machinery through the mediator complex (Kagey et al., 2010) or by organizing chromatin structure (Zuin et al., 2014).

Rad21 associates with the core promoters/TSSs of known key stem cell markers and Wnt target genes that are critical for CRC. Of particular interest is the association of Rad21 with the *Lgr5* ISC gene. This association appears to have a direct and positive role for Rad21 in regulating *Lgr5*, since a specific reduction of *Lgr5* mRNA was observed in *Rad21*<sup>+/−</sup> animals. Further, this regulatory role of Rad21 for *Lgr5* is likely to be functionally significant in that it affects ISC activity. Although the self-renewal of primary organoids was unaffected by *Rad21* heterozygosity, our previous *in vivo* assay showed that ISC potential was compromised by *Rad21* haploinsufficiency following ionizing radiation (Xu et al., 2010). Importantly, we found that the self-renewal of cyst-like organoids was severely compromised by *Rad21* heterozygosity. In view of our data that the majority of cyst-like organoids had already lost the WT *Apc* allele, the effect of *Rad21* haploinsufficiency on ISC activity is likely to be Wnt dependent. Furthermore, Rad21 expression in Paneth cells is likely to affect the interdigitated *Lgr5*<sup>+</sup> ISCs, since Paneth cells are essential components of the ISC niche and their deletion resulted in the loss of *Lgr5*<sup>+</sup> cells (Akcora et al., 2013; Sato et al., 2011). This is, however, likely to be indirect, possibly through Wnt signaling, as it is at its strongest in Paneth cells (van Es et al., 2005). Since *Lgr5*<sup>+</sup> stem cell-specific loss of *Apc* (i.e., the activation of Wnt signaling) was shown to be essential for the initiation and progression of adenomagenesis (Barker et al., 2009), our findings support an interplay between *Rad21* and *Lgr5* in the early stage of adenomagenesis in the context of

Wnt signaling. Our data that Rad21 associates with the promoters of multiple Wnt target genes further support a direct regulatory role for Rad21 in the Wnt signaling pathway, which in turn promotes neoplastic transformation.

### **Rad21 Association with Retrotransposons as a Mechanism for Inducing Genomic Instability and Transcriptional Dysregulation in Adenomas**

Retrotransposons are mobile genetic elements that are potent endogenous mutagens and are kept in an inactive state. The transcription of retrotransposons and the subsequent insertion, primarily with L1, into new sites has been reported in human cancers and can lead to disruption of TSGs (Lee et al., 2012), activation of proto-oncogenes (Nigumann et al., 2002), as well as the genesis of large genomic rearrangements (Mazoyer, 2005). Our ChIP-seq analysis provides evidence that Rad21 and/or cohesin is an important regulator of these repetitive mobile DNA sequences, in particular L1. We found that RAD21 expression directly affects the *L1*-promoter activity *in vitro* and that Rad21 association with the *L1* promoter is independent of methylation, a known mechanism controlling the *L1* activity (Iskow et al., 2010). We thus propose that Rad21 and/or cohesin exerts both direct and indirect effects on the *L1* activities, by either directly driving *L1* expression, or by mediating the formation of chromatin loops.

Our data revealed a strong association between *L1* expression and elevated RAD21 expression in human CRCs, implicating RAD21-mediated *L1* expression in CRC carcinogenesis and prognosis. *L1*-encoded reverse transcriptase activity is implicated in driving cellular transformation (Patnala et al., 2014). RAD21-mediated *L1* expression might contribute to this process. The ability of *L1* transcripts in autonomous retrotransposition could potentially lead to the disruption of gene expression in CRCs that have been shown to have the highest frequency of *L1* somatic insertions (Lee et al., 2012). Another possible consequence for RAD21-L1 interaction is in inducing CIN. Retrotransposons, once transcriptionally unsilenced, are then freed to mobilize throughout the genome and engage in HR, both locally and globally (Iskow et al., 2010; Nigumann et al., 2002). Such illegitimate recombination events between repetitive elements spanning the genome are likely to serve CIN. Elevated RAD21 expression may promote hyperrecombination of such repetitive elements. Finally, *L1* promoter methylation was reported to be a potential prognostic marker in gastrointestinal cancer (Baba et al., 2014). In view of our finding that Rad21-mediated *L1* expression is independent of *L1* methylation, it would be of interest to evaluate the prognostic value of *L1* expression in the context of Rad21 expression.

### **Role of Cohesin in Tumorigenesis**

We propose that Rad21 contributes to the early events that are essential for the initiation and progression of adenomas through

(C) Enrichment for Rad21 at the 5' upstream regions (blue boxed regions) and TSS (red boxed region) of the *Lgr5* gene. Left: Rad21 enrichment in adenomas revealed by ChIP-seq. Left: relative Rad21 enrichment confirmed by ChIP-qPCR.

(D) Rad21 enrichment at the upstream and TSS of the cohesin *Smc3* gene.

(E) A negative control region on chromosome 17 showing no Rad21 enrichment.

ChIP-qPCR data represent mean  $\pm$  SEM of three independent ChIP assays. \*p < 0.05; ns, not significant. See also Figure S5.

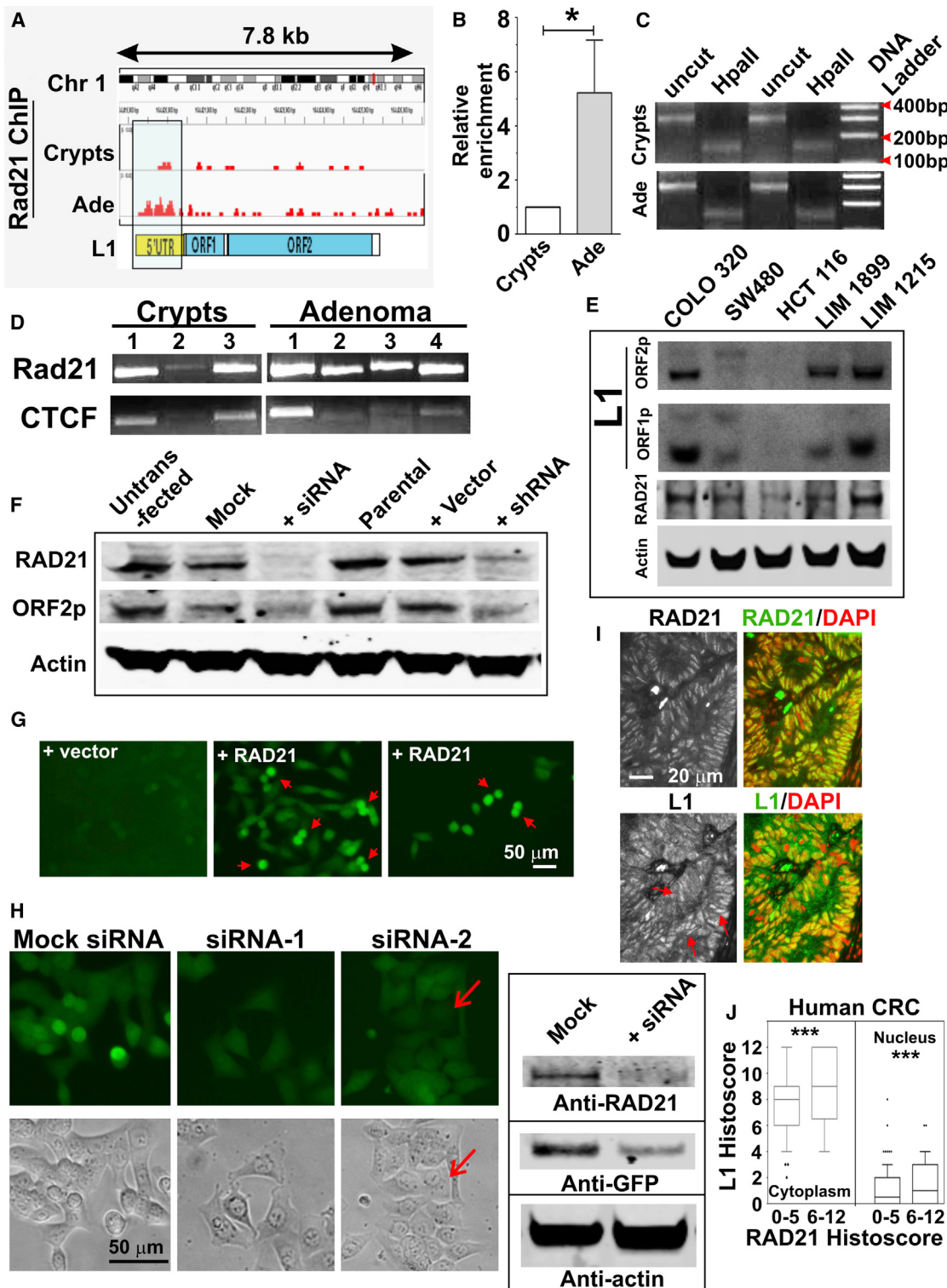


**Figure 7.** Rad21 Binding to L1 Retrotransposon 5' UTR Regions in *Apc<sup>Min/+</sup>* Adenomas and Its Activated Expression in Human CRC Cell Lines, Sporadic Adenomas, and CRC

(A) Enriched (boxed regions) Rad21 binding to the internal promoter within the 5' UTR tandem repeats of L1. Ade, adenomas.

(B) ChIP-qPCR showing increased Rad21 binding in the 5' UTR of L1 elements. Data represent mean ± SEM of three independent ChIP assays. \*p < 0.05.

(legend continued on next page)

multiple mechanisms. Our findings suggest RAD21 as a driver of an insidious cycle of genomic instability, first through promoting *Apc* LOH, which in turn upregulates *Rad21* expression, which further drives global genomic instability via the Wnt signaling pathway and retrotransposon activation. These mechanisms are not inherently restricted to intestinal carcinogenesis, and the findings of this study raise a number of questions as to the broader implications of cohesin dysregulation in other human cancers.

## EXPERIMENTAL PROCEDURES

### Mice and Cell Lines

*Apc*<sup>Min/+</sup> mice (Moser et al., 1992) were crossed with *Rad21*<sup>+/−</sup> mice (Xu et al., 2010) on a C57BL/6J background under specific-pathogen-free conditions. All experiments were conducted with approvals by the Institutional Animal Ethics committee (E389 and E470). Human CRC cell lines and cell culture conditions are described in the [Supplemental Experimental Procedures](#).

### Organoid Culture

Primary organoids were established from isolated SI crypts as described previously (Sato et al., 2009; Xu et al., 2010). To establish secondary organoid cultures, primary organoids were disaggregated to single cells and reseeded in Matrigel containing Rho-kinase inhibitor (Y-27632; Sigma-Aldrich).

### *Apc* LOH Assay

Individual organoids were picked from primary cultures, and PCR products were digested with Hind III (Promega) and separated on 10% polyacrylamide gels (Amrasco). Signal intensity was measured using Image One software (Bio-Rad).

### Mitoses, Chromosome Spreads, and SCEs

Mitosis, aneuploidy, and SCE were scored essentially as described previously (Xu et al., 2010). For SCEs, bromodeoxyuridine (BrdU) was added at 5 μM for 48 hr and MMC at 6 μM for 30 min prior to the addition of Colcemid.

### DR-GFP Recombination Assay

HCT116 cells were transfected with DR-GFP DNA and selected for puromycin-resistant clones. A total of 20 μM of RAD21 siRNA (SMARTpool ON-Target Plus) was delivered using DharmaFECT 2 (DF2; GE Healthcare Dharmacon). Controls are cells treated with either Opti-MEM or mock transfected without siRNA. Cells were analyzed 48 hr after pCβASce transfection with a FACS Diva II (BD Biosciences). Data from two independent experiments, each with three independent transfections, were analyzed using Flowlogic software.

### qRT-PCR

qRT-PCR was performed using SYBG master mix (Applied Biosystems), and primers are listed in [Table S7](#). Each data point represents a minimum of three animals per genotype and three independent harvests for human cell lines.

- (C) L1 promoter methylation analysis of a ~300 bp fragment encompassing CpG islands at the 5' UTR. The presence of a smaller fragment following HpaII digestion indicates unmethylated DNA. DNA from two independent Rad21 ChIP assays for each tissue was used. Ade, adenoma.
  - (D) PCR showing Rad21 and CTCF colocalization at individual L1 loci.
  - (E) Western blots of L1 and RAD21 expression in human CRC cell lines. L1 mRNA contains two ORFs, ORF1 and ORF2. Actin, loading control.
  - (F) Western blots showing an apparent reduction in L1 expression following siRNA and shRNA-mediated RAD21 KD in LIM1215 cells.
  - (G) Stable L1-GFP expression in HCT116 cells with enforced RAD21 expression and the vector control. Identical exposure for all images. Note the stronger GFP signal in doublets (arrows).
  - (H) The effect of L1-GFP expression following siRNA knockdown of RAD21 in HCT116 cells. Note the reduced GFP signal in siRNA-transfected cells. In some cases, GFP signal is mostly lost (arrows). Identical exposures for GFP images. Left: western blots validating the expression of RAD21 and the GFP reporter.
  - (I) IF of RAD21 (top) and L1 (bottom) on adjacent sections. Monochrome images in black and white. Rad21 or L1 (green) and DNA (red) colocalization (yellow) in merged images. RAD21 staining is homogenous and predominantly nuclear. L1 expression is predominantly cytoplasmic and, in some cases, in the nucleus (red arrows).
  - (J) Cytoplasmic or nuclear L1 expression corresponds to elevated RAD21 expression in human CRC. n = 142 cases. \*\*\*p < 0.001.
- See also [Figure S6](#).

### Immunofluorescence and Immunohistochemistry

Immunofluorescence of cells was performed as described previously (Xu et al., 2004) on paraffin-embedded sections following irradiation with a UV transilluminator. IHC was performed as described previously (Xu et al., 2011b). CRC ethic approvals were CO2.216 (Oxford cohort) and St Vincent's Hospital HREC H00/022 (Sydney cohort). CRC cases were assembled as TMA with duplicate tumor cores per case.

### Cell Cycle and Proliferation

Cells were pulse-labeled with 5 mM BrdU (Sigma-Aldrich) and stained with anti-BrdU (BD Biosciences) (Deardorff et al., 2012). Flow cytometry used a FACS Diva II (BD Biosciences). Cell-cycle profiles were analyzed using Flowlogic software. Cell proliferation assays were done as described previously (Xu et al., 2011b).

### Human L1-GFP Expression Analysis

The 1.35 kb human L1 5' UTR-enhanced GFP construct was transfected into HCT116 p53<sup>−/−</sup> cells. GFP-positive cells were sorted to 99% purity using fluorescence-activated cell sorting. Cells were imaged using an inverted microscope (Leica) or harvested for protein analysis following siRNA delivery.

### RNA-Seq and ChIP-Seq

For RNA-seq, 50 bp pair-end sequencing was performed on the Hi-seq 2500 system (Illumina). ChIP was carried out using a ChIP validated rabbit anti-Rad21 (Ab992, Abcam) and 50 bp single-end sequencing performed on the Hi-seq 2000 system (Illumina). Short reads were mapped to mouse genome reference UCSC MM9. Data analyses are described in the [Supplemental Experimental Procedures](#).

### L1 Promoter Methylation Analysis by HpaII Restriction Digestion

DNA corresponding to either ~240 bp mouse L1 5' UTR tandem repeats or the 5' UTR of individual L1 loci were amplified by PCR following Rad21 ChIP and digested with HpaII (Promega). Primers are listed in [Table S8](#).

### ALDEFLUOR Assay

Single-cell suspensions from SI crypts were stained using ALDEFLUOR stem cell detection kit (STEMCELL Technologies) and sorted with FACS Diva (BD Biosciences).

### Statistical Analyses

Kaplan-Meier survival curves were compared using the log rank test. Fisher's exact test was performed for adenoma frequency, LOH and aneuploidy using R software version 2.15.0 (<http://www.r-project.org>). Student's t test was performed for all other analyses.

### ACCESSION NUMBERS

Data sets were deposited to the NCBI Gene Expression Omnibus under the accession number GSE59283.

**SUPPLEMENTAL INFORMATION**

Supplemental Information includes Supplemental Experimental Procedures, six figures, and eight tables and can be found with this article online at <http://dx.doi.org/10.1016/j.celrep.2014.10.059>.

**AUTHOR CONTRIBUTIONS**

H.X. and R.G.R. designed the project; H.X. performed most experiments and analyzed data; Y.Y. performed animal survival, tumor incidence, AOM, CAT, SCE, and mitosis experiments; and S.D., R.L.W., N.L.H., N.J.M., S.B.F., and M.J.M. contributed to human TMA work. N.E.C. scored and analyzed RAD21/Ki-67 coimmunofluorescence. Other contributions include D.R. and L.C. to L1 work, M.G. and J.M. to organoid and ISC activity assays, and R.W.T. to ChIP-seq. H.X., M.J.M., and R.G.R. wrote the manuscript.

**ACKNOWLEDGMENTS**

The NHMRC provided program and project grant support to R.G.R., H.X., and M.J.M. We thank Dr. Maria Jasin for providing DR-GFP plasmids, Dr. Elaine Sanij for discussion on ChIP-seq, Aga Borcz and Tim Holloway for ChIP and RNA library preparation, Drs. Jason Ellul and Jason Li for assisting in bioinformatics, Drs. Olga Martin and Delphine Denoyer for advice on DSB immunofluorescence, Patricia Bukczynska for discussion on siRNA transfection, and Dr. Maree Faux for advice on Apc western analysis. We also thank the Flow Cytometry Core for fluorescence-activated cell sorting and the Microscopy Core for assistance with histology and image collection and Cassie Bush and Chantelle Newman for animal husbandry.

Received: February 3, 2014

Revised: August 29, 2014

Accepted: October 27, 2014

Published: November 20, 2014

**REFERENCES**

- Akcora, D., Huynh, D., Lightowler, S., Germann, M., Robine, S., de May, J.R., Pollard, J.W., Stanley, E.R., Malaterre, J., and Ramsay, R.G. (2013). The CSF-1 receptor fashions the intestinal stem cell niche. *Stem Cell Res. (Amst.)* **10**, 203–212.
- Baba, Y., Murata, A., Watanabe, M., and Baba, H. (2014). Clinical implications of the LINE-1 methylation levels in patients with gastrointestinal cancer. *Surg. Today* **44**, 1807–1816.
- Barber, T.D., McManus, K., Yuen, K.W., Reis, M., Parmigiani, G., Shen, D., Barrett, I., Nouhi, Y., Spencer, F., Markowitz, S., et al. (2008). Chromatid cohesion defects may underlie chromosome instability in human colorectal cancers. *Proc. Natl. Acad. Sci. USA* **105**, 3443–3448.
- Barker, N., Ridgway, R.A., van Es, J.H., van de Wetering, M., Begthel, H., van den Born, M., Danenbergh, E., Clarke, A.R., Sansom, O.J., and Clevers, H. (2009). Crypt stem cells as the cells-of-origin of intestinal cancer. *Nature* **457**, 608–611.
- Caldwell, C.M., Green, R.A., and Kaplan, K.B. (2007). APC mutations lead to cytokinetic failures in vitro and tetraploid genotypes in Min mice. *J. Cell Biol.* **178**, 1109–1120.
- Clevers, H., and Nusse, R. (2012). Wnt/β-catenin signaling and disease. *Cell* **149**, 1192–1205.
- Cottrell, S., Bicknell, D., Kaklamani, L., and Bodmer, W.F. (1992). Molecular analysis of APC mutations in familial adenomatous polyposis and sporadic colon carcinomas. *Lancet* **340**, 626–630.
- Deardorff, M.A., Wilde, J.J., Albrecht, M., Dickinson, E., Tennstedt, S., Braunholz, D., Mönnich, M., Yan, Y., Xu, W., Gil-Rodríguez, M.C., et al. (2012). RAD21 mutations cause a human cohesinopathy. *Am. J. Hum. Genet.* **90**, 1014–1027.
- Deb, S., Xu, H., Tuynman, J., George, J., Yan, Y., Li, J., Ward, R.L., Mortensen, N., Hawkins, N.J., McKay, M.J., et al. (2014). RAD21 cohesin overexpression is a prognostic and predictive marker exacerbating poor prognosis in KRAS mutant colorectal carcinomas. *Br. J. Cancer* **110**, 1606–1613.
- Dikovskaya, D., Schiffmann, D., Newton, I.P., Oakley, A., Kroboth, K., Sansom, O., Jamieson, T.J., Meniel, V., Clarke, A., and Nähthke, I.S. (2007). Loss of APC induces polyploidy as a result of a combination of defects in mitosis and apoptosis. *J. Cell Biol.* **176**, 183–195.
- Dorsett, D. (2011). Cohesin: genomic insights into controlling gene transcription and development. *Curr. Opin. Genet. Dev.* **21**, 199–206.
- Faux, M.C., Ross, J.L., Meeker, C., Johns, T., Ji, H., Simpson, R.J., Layton, M.J., and Burgess, A.W. (2004). Restoration of full-length adenomatous polyposis coli (APC) protein in a colon cancer cell line enhances cell adhesion. *J. Cell Sci.* **117**, 427–439.
- Fleming, E.S., Temchin, M., Wu, Q., Maggio-Price, L., and Tirnauer, J.S. (2009). Spindle misorientation in tumors from APC(min+) mice. *Mol. Carcinog.* **48**, 592–598.
- Guillou, E., Ibarra, A., Coulon, V., Casado-Vela, J., Rico, D., Casal, I., Schwob, E., Losada, A., and Méndez, J. (2010). Cohesin organizes chromatin loops at DNA replication factories. *Genes Dev.* **24**, 2812–2822.
- Haering, C.H., Farca, A.M., Arumugam, P., Metson, J., and Nasmyth, K. (2008). The cohesin ring concatenates sister DNA molecules. *Nature* **454**, 297–301.
- Haigis, K.M., and Dove, W.F. (2003). A Robertsonian translocation suppresses a somatic recombination pathway to loss of heterozygosity. *Nat. Genet.* **33**, 33–39.
- Iskow, R.C., McCabe, M.T., Mills, R.E., Torene, S., Pittard, W.S., Neuwald, A.F., Van Meir, E.G., Vertino, P.M., and Devine, S.E. (2010). Natural mutagenesis of human genomes by endogenous retrotransposons. *Cell* **141**, 1253–1261.
- Jessberger, R. (2009). Cohesin's dual role in the DNA damage response: repair and checkpoint activation. *EMBO J.* **28**, 2491–2493.
- Johnson, D.S., Mortazavi, A., Myers, R.M., and Wold, B. (2007). Genome-wide mapping of in vivo protein-DNA interactions. *Science* **316**, 1497–1502.
- Kagey, M.H., Newman, J.J., Bilodeau, S., Zhan, Y., Orlando, D.A., van Berkum, N.L., Ebmeier, C.C., Goossens, J., Rahl, P.B., Levine, S.S., et al. (2010). Mediator and cohesin connect gene expression and chromatin architecture. *Nature* **467**, 430–435.
- Kong, X., Ball, A.R., Jr., Sonoda, E., Feng, J., Takeda, S., Fukagawa, T., Yen, T.J., and Yokomori, K. (2009). Cohesin associates with spindle poles in a mitosis-specific manner and functions in spindle assembly in vertebrate cells. *Mol. Biol. Cell* **20**, 1289–1301.
- Lee, E., Iskow, R., Yang, L., Gokcumen, O., Haseley, P., Luquette, L.J., 3rd, Lohr, J.G., Harris, C.C., Ding, L., Wilson, R.K., et al.; Cancer Genome Atlas Research Network (2012). Landscape of somatic retrotransposition in human cancers. *Science* **337**, 967–971.
- Mazoyer, S. (2005). Genomic rearrangements in the BRCA1 and BRCA2 genes. *Hum. Mutat.* **25**, 415–422.
- McKay, M.J., Troelstra, C., van der Spek, P., Kanaar, R., Smit, B., Hagemeijer, A., Bootsma, D., and Hoeijmakers, J.H. (1996). Sequence conservation of the rad21 Schizosaccharomyces pombe DNA double-strand break repair gene in human and mouse. *Genomics* **36**, 305–315.
- Møllersen, L., Paulsen, J.E., and Alexander, J. (2004). Loss of heterozygosity and nonsense mutation in Apc in azoxymethane-induced colonic tumours in min mice. *Anticancer Res.* **24** (5A), 2595–2599.
- Moreb, J.S. (2008). Aldehyde dehydrogenase as a marker for stem cells. *Curr. Stem Cell Res. Ther.* **3**, 237–246.
- Moser, A.R., Dove, W.F., Roth, K.A., and Gordon, J.I. (1992). The Min (multiple intestinal neoplasia) mutation: its effect on gut epithelial cell differentiation and interaction with a modifier system. *J. Cell Biol.* **116**, 1517–1526.
- Moynahan, M.E., and Jasin, M. (2010). Mitotic homologous recombination maintains genomic stability and suppresses tumorigenesis. *Nat. Rev. Mol. Cell Biol.* **11**, 196–207.

- Nasmyth, K. (2001). Disseminating the genome: joining, resolving, and separating sister chromatids during mitosis and meiosis. *Annu. Rev. Genet.* 35, 673–745.
- Nigumann, P., Redik, K., Mätlik, K., and Speek, M. (2002). Many human genes are transcribed from the antisense promoter of L1 retrotransposon. *Genomics* 79, 628–634.
- Patnala, R., Lee, S.H., Dahlstrom, J.E., Ohms, S., Chen, L., Dheen, S.T., and Rangasamy, D. (2014). Inhibition of LINE-1 retrotransposon-encoded reverse transcriptase modulates the expression of cell differentiation genes in breast cancer cells. *Breast Cancer Res. Treat.* 143, 239–253.
- Pierce, A.J., Johnson, R.D., Thompson, L.H., and Jasins, M. (1999). XRCC3 promotes homology-directed repair of DNA damage in mammalian cells. *Genes Dev.* 13, 2633–2638.
- Rhodes, J.M., Bentley, F.K., Print, C.G., Dorsett, D., Misulovin, Z., Dickinson, E.J., Crosier, K.E., Crosier, P.S., and Horsfield, J.A. (2010). Positive regulation of c-Myc by cohesin is direct, and evolutionarily conserved. *Dev. Biol.* 344, 637–649.
- Sato, T., Vries, R.G., Snippert, H.J., van de Wetering, M., Barker, N., Stange, D.E., van Es, J.H., Abo, A., Kujala, P., Peters, P.J., and Clevers, H. (2009). Single Lgr5 stem cells build crypt-villus structures in vitro without a mesenchymal niche. *Nature* 459, 262–265.
- Sato, T., van Es, J.H., Snippert, H.J., Stange, D.E., Vries, R.G., van den Born, M., Barker, N., Shroyer, N.F., van de Wetering, M., and Clevers, H. (2011). Paneth cells constitute the niche for Lgr5 stem cells in intestinal crypts. *Nature* 469, 415–418.
- Schaaf, C.A., Misulovin, Z., Gause, M., Koenig, A., Gohara, D.W., Watson, A., and Dorsett, D. (2013). Cohesin and polycomb proteins functionally interact to control transcription at silenced and active genes. *PLoS Genet.* 9, e1003560.
- Sonoda, E., Sasaki, M.S., Morrison, C., Yamaguchi-Iwai, Y., Takata, M., and Takeda, S. (1999). Sister chromatid exchanges are mediated by homologous recombination in vertebrate cells. *Mol. Cell. Biol.* 19, 5166–5169.
- Spirio, L.N., Samowitz, W., Robertson, J., Robertson, M., Burt, R.W., Leppert, M., and White, R. (1998). Alleles of APC modulate the frequency and classes of mutations that lead to colon polyps. *Nat. Genet.* 20, 385–388.
- van Es, J.H., Jay, P., Gregorjeff, A., van Gijn, M.E., Jonkheer, S., Hatzis, P., Thiele, A., van den Born, M., Begthel, H., Brabetz, T., et al. (2005). Wnt signaling induces maturation of Paneth cells in intestinal crypts. *Nat. Cell Biol.* 7, 381–386.
- Wong, R.W., and Blobel, G. (2008). Cohesin subunit SMC1 associates with mitotic microtubules at the spindle pole. *Proc. Natl. Acad. Sci. USA* 105, 15441–15445.
- Xu, H., Beasley, M., Verschoor, S., Inselman, A., Handel, M.A., and McKay, M.J. (2004). A new role for the mitotic RAD21/SCC1 cohesin in meiotic chromosome cohesion and segregation in the mouse. *EMBO Rep.* 5, 378–384.
- Xu, H., Balakrishnan, K., Malaterre, J., Beasley, M., Yan, Y., Essers, J., Appeldoorn, E., Tomaszewski, J.M., Vazquez, M., Verschoor, S., et al. (2010). Rad21-cohesin haploinsufficiency impedes DNA repair and enhances gastrointestinal radiosensitivity in mice. *PLoS ONE* 5, e12112.
- Xu, H., Tomaszewski, J.M., and McKay, M.J. (2011a). Can corruption of chromosome cohesion create a conduit to cancer? *Nat. Rev. Cancer* 11, 199–210.
- Xu, H., Yan, M., Patra, J., Natrajan, R., Yan, Y., Swagemakers, S., Tomaszewski, J.M., Verschoor, S., Millar, E.K., van der Spek, P., et al. (2011b). Enhanced RAD21 cohesin expression confers poor prognosis and resistance to chemotherapy in high grade luminal, basal and HER2 breast cancers. *Breast Cancer Res.* 13, R9.
- Yan, M., Xu, H., Waddell, N., Shield-Artin, K., Haviv, I., McKay, M.J., and Fox, S.B.; kConFab authors (2012). Enhanced RAD21 cohesin expression confers poor prognosis in BRCA2 and BRCA1, but not BRCA1 familial breast cancers. *Breast Cancer Res.* 14, R69.
- Zhang, J., Neisa, R., and Mao, Y. (2009). Oncogenic Adenomatous polyposis coli mutants impair the mitotic checkpoint through direct interaction with Mad2. *Mol. Biol. Cell* 20, 2381–2388.
- Zuin, J., Dixon, J.R., van der Reijden, M.I., Ye, Z., Kolovos, P., Brouwer, R.W., van de Corput, M.P., van de Werken, H.J., Knoch, T.A., van IJcken, W.F., et al. (2014). Cohesin and CTCF differentially affect chromatin architecture and gene expression in human cells. *Proc. Natl. Acad. Sci. USA* 111, 996–1001.